JOC The Journal of Organic Chemistry

Article

pubs.acs.org/joc

The Decarboxylation of α,β-Unsaturated Acid Catalyzed by Prenylated FMN-Dependent Ferulic Acid Decarboxylase and the Enzyme Inhibition

Cui-Lan Lan and Shi-Lu Chen*

Key Laboratory of Cluster Science of Ministry of Education, School of Chemistry and Chemical Engineering, Beijing Institute of Technology, Beijing 100081, China

Supporting Information

ABSTRACT: Ferulic acid decarboxylase (Fdc1) is able to catalyze the decarboxylation of α,β-unsaturated acids using a novel cofactor, prenylated flavin mononucleotide (PrFMN). Using density functional theory calculations, we here have investigated the Fdc1 reaction mechanism with the substrate of α-methylcinnamic acid. It is demonstrated that Fdc1 employs a 1,3-dipolar cycloaddition mechanism involving four concerted steps, where the Glu282 acts as a crucial proton donor to protonate the α carbon (C_α). The last step, the decomposition of a pyrrolidine species, is rate-limiting with an overall barrier of 18.9 kcal mol^{-1}. Furthermore, when α-hydroxycinnamic acid is used, the Glu282 is found to have another face to transport the hydroxyl proton to the C_β atom to promote the tautomerization from enol intermediate to ketone species leading to the inhibition of the Fdc1 enzyme. The PrFMN roles are also discussed in detail.

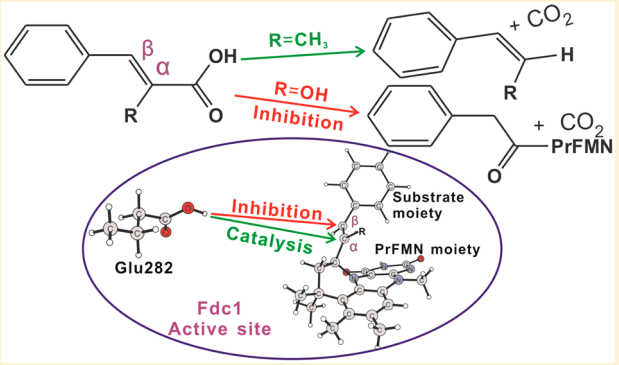

INTRODUCTION

Decarboxylases play important roles in the synthesis of alcohols, carboxylic acids, terminal olefins, and other important chemicals under very mild reaction conditions.[1] For instance, decarboxylases provide a sustainable and environment-friendly approach to synthesize styrene directly from renewable resources, such as glucose.[2] The styrene, acting as a monomer building block for many useful polymers, is an important basis material for the petrochemical industry. However, now all commercial styrene is obtained from the dwindling petroleum resources.

The biosynthesis of styrene is achieved from the enzymatic decarboxylation of α,β-unsaturated acid via the coexpression of Fdc1 (ferulic acid decarboxylase) and Pad1 (phenylacrylic acid decarboxylase) (Figure 1A).[3−6] The UbiD and UbiX enzymes[7,8] were found to be the homologues of Fdc1 and Pad1, respectively, and are involved in the decarboxylation of 3-polyprenyl-4-hydroxybenzoate (Figure 1A), an intermediate in ubiquinone (coenzyme Q) biosynthesis.[9−11]

It has been shown that the removal of either of the two genes (Fdc1 and Pad1) drastically reduces the decarboxylase activity.[4,5] Recent studies revealed that Fdc1/UbiD essentially catalyzes the decarboxylation via a previously unknown cofactor, prenylated flavin mononucleotide (PrFMN) (Figure 1B), while Pad1/UbiX is responsible for the formation of PrFMN.[12−14] Fdc1-catalyzed decarboxylation of α,β-unsaturated acids was found to be reversible, making it possible to be utilized in the fixation of carbon dioxide.[12] Interestingly, when the substrate α-position was substituted by a hydroxyl, that is, α-hydroxycinnamic acid (the enol tautomer of phenylpyruvate) was used, the Fdc1 enzyme was inhibited (Figure 2).[12] With this, the characterization of the particularly novel PrFMN cofactor and the mechanistic investigations of the Fdc1 reaction and its inhibition are thus of great importance for the understanding of this new piece in enzymatic decarboxylation and may benefit styrene biosynthesis and CO_2 fixation.

In the present work, using the density functional theory (DFT) with the hybrid functional B3LYP,[15−17] we have studied the reaction and inhibition mechanisms of Fdc1 with a chemical model (Figure 1B) constructed on the basis of an X-ray crystal structure (PDB ID: 4ZA7).[12] We present the energetics and provide the characterization of stationary points involved. The calculations have demonstrated that Fdc1 employs a 1,3-dipolar cycloaddition mechanism (Figure 2)[12,18,19] and in particular reveal the interesting bifunctional roles of Glu282 in catalysis and inhibition. The roles of the novel PrFMN cofactor have also been analyzed in detailed.

COMPUTATIONAL METHODS

All calculations were performed using the DFT with the hybrid functional B3LYP[15−17] as implemented in the Gaussian 09 D01 program package.[20] Geometry optimizations were carried out

Received: August 2, 2016
Published: September 12, 2016

DOI: 10.1021/acs.joc.6b01872
J. Org. Chem. 2016, 81, 9289−9295

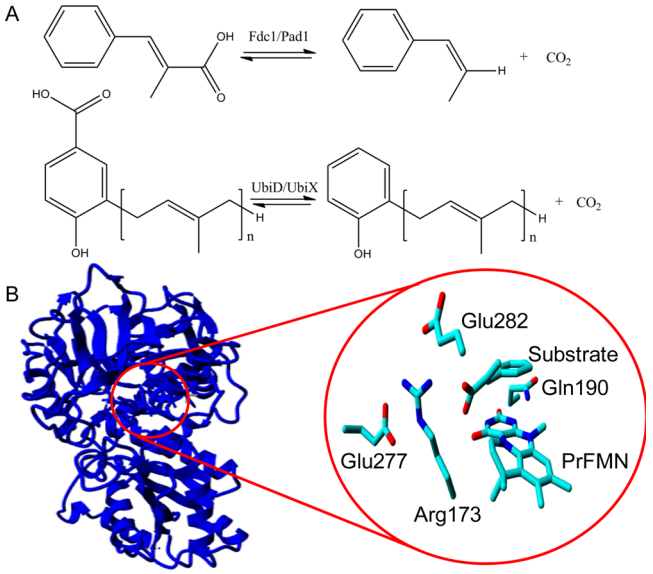

Figure 1. Decarboxylation reactions catalyzed by Fdc1/Pad1 and UbiD/UbiX (A), and overall view of Fdc1 and close-up view of its active site (B). Coordinates from PDB entry 4ZA7[12] were used to generate the figures.

with the 6-31G(d,p) basis set for all atoms.[21,22] On the basis of the optimized geometries, more accurate energies were obtained by performing single-point calculations with a larger basis set 6-311+G(2d,2p) for all elements. Frequency calculations were performed at the same theory level as the optimizations to obtain zero-point energies and to further confirm the nature of the stationary points. The solvation effects of the protein environment on the calculated energies were estimated at the same theory level as the optimizations by performing single-point calculations on the optimized structures using a homogeneous dielectric field according to the CPCM method.[23−26] The dielectric constant (ε) was chosen to be 4, which is a standard value used in many previous studies.[27−29] Dispersion has been revealed to be significant in a few cases, including dicopper complexes,[30,31] cobalamin-dependent enzymes,[30,32,33] and isoaspartyl dipeptidase.[34] In the present work on Fdc1, an enzyme that may involve π-stacking interactions in its active site, dispersion corrections were included in both geometry optimizations and energy evaluation using the empirical formula by Grimme et al. (i.e., DFT-D3).[35−38] As described below, a few atoms were frozen to their crystal positions. An investigation with acetylene hydratase as an example[39] indicates that the coordinate error of varying constraints has a very small effect on the calculated energies when the resolution of the starting crystal structure is better than 2.0 Å (1.10 Å in this case of Fdc1).[12] Another study of phosphotriesterase[40] also shows that the energy differences between with and without atom locking do not alter any conclusion about the mechanism. However, the fixation of a few atoms would make the calculation of harmonic entropy effects inaccurate. It is thus still very difficult to accurately calculate entropy. Fortunately, in most cases the entropy effects are not of such a magnitude that they will change conclusions about the mechanism. In the present work, the attempts to estimate entropy have been made by excluding the contributions of frozen atoms to vibrational frequencies. As described later, the energetics with this kind of entropy corrected (given in Figures S1 and S2 in the Supporting Information) are basically consistent with the ones without entropy, especially in the forward reaction and the comparison of competing pathways. Therefore, the energetics without entropy corrections are presented in the text. If not otherwise indicated, all

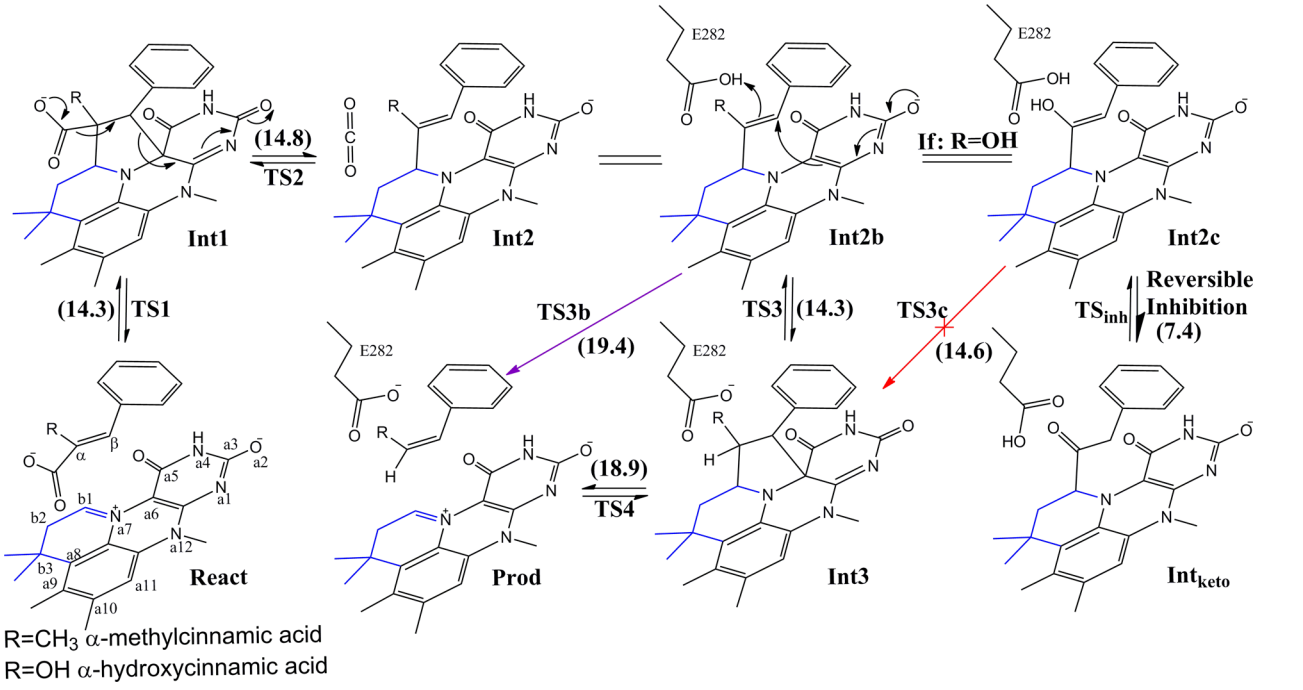

Figure 2. Reaction mechanism of Fdc1 hypothesized by Payne et al.[12] and the enzyme inhibition. The pathway indicated by the red arrow is demonstrated to be inaccessible in this work, while the purple pathway is shown to be a little unfavorable but still competing. The prenyl moiety in the PrFMN cofactor is shown in blue. α-Hydroxycinnamic acid is the enol tautomer of phenylpyruvate. Energy barriers in the forward direction are given in the parentheses with the unit of kcal mol^{-1}.

DOI: 10.1021/acs.joc.6b01872
J. Org. Chem. 2016, 81, 9289−9295

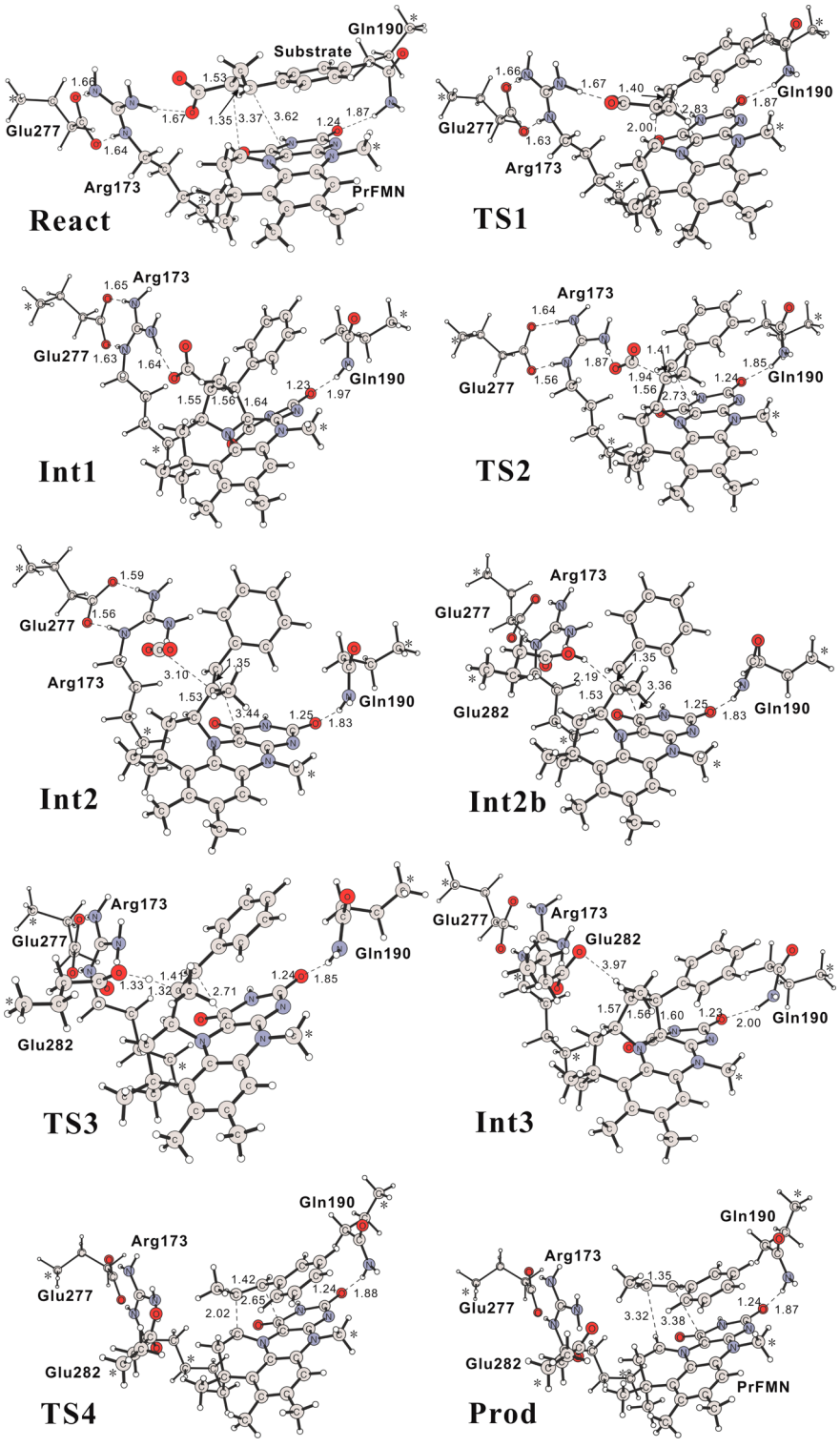

Figure 3. Optimized structures of stationary points in the Fdc1-catalyzed decarboxylation of α-methylcinnamic acid. All distances are in angstroms (Å). Asterisks indicate the atoms that are fixed to their crystal positions.

energies offered in this paper have been corrected by dispersion effects, zero-point energies, and solvation effects, but not by entropy effects. The energetics with entropy corrected are given in the Supporting Information (Figures S1 and S2). The present procedure of cluster modeling has been carefully benchmarked[27,29,34,36,41] and well reviewed.[27,29,42,43] It has been successfully applied to a large number of enzymes by different research groups.[27,29,42,44−59] In addition, Cartesian coordinates of optimized structures are given in the Supporting Information.

RESULTS AND DISCUSSION

Chemical Model. A chemical model was constructed based on the crystal structure of Fdc1 with the substrate of α-methylcinnamic acid and the PrFMN cofactor bound (PDB ID: 4ZA7).[12] With this crystal structure, we can obtain an initial

DOI: 10.1021/acs.joc.6b01872
J. Org. Chem. 2016, 81, 9289−9295

geometry of the enzyme−substrate−cofactor complex which truly reflects their relative positions. It has been shown that the R173A, E277Q, and E282Q mutants of Fdc1 are all inactive,[12] which indicates that these residues are critical for the decarboxylation. Gln190 is observed to have electrostatic interactions with a cofactor carbonyl.[12] Therefore, besides the substrate (α-methylcinnamic acid) and the PrFMN cofactor, the four residues (Glu282, Arg173, Glu277, and Gln190) were included in the model (Figure 1B). To reduce the size, some truncations were made so that only the side chains of residues were involved in the model. To preserve the spatial arrangement of the residues, the atoms where the truncations were made were fixed to their crystal positions.

Using the PROPKA 3.1 program developed by Jensen et al.[60−63] and the crystal structure of 4ZA7,[12] the pK_a's of Glu282, Glu277, and Arg173 are estimated to be 6.40, 4.05, and 19.53 respectively. Since the Fdc1 reaction was carried out at pH = 6,[12] the Glu282 and Glu277 in the model are presented in the protonation and deprotonation states, respectively. The Arg173 residue is also protonated. In addition, the substrate carboxylate is deprotonated. It should be mentioned that, to reduce computational consumption and conformational uncertainty, the Glu282 was included in the model only after the decarboxylation step, while the CO_2 molecule was excluded from the model once it has been formed.

The geometrical parameters obtained from the optimization of this model agree well with the crystal strucutre. In particular, in the optimized enzyme−substrate−cofactor complex (denoted by **React**, Figure 3) the substrate is orientated by the Arg173 via hydrogen bonding, guiding its π-stacking with the cofactor plane. As a result, the key reacting atoms proposed in Figure 2 are located reasonably. For example, the distance between the substrate C_α and the cofactor C_{b1} is 3.37 Å while the C_β−C_{a6} distance is 3.62 Å (see **React** in Figure 3).

Reaction Mechanism of Fdc1 with α-Methylcinnamic Acid. The first step in the Fdc1 reaction was proposed by Payne et al.[12] to be the 1,3-dipolar cycloaddition via the C_α−C_{b1} and C_β−C_{a6} couplings to form a pyrrolidine intermediate (Figure 2). To speculate the likely reacting sites, the electrostatic potential (ESP) surfaces for the substrate and cofactor were constructed (Figure 4). From Figure 4, it can be observed that the C_{b1} atom in the prenyl moiety has the lowest electron density among the unsaturated atoms in the PrFMN cofactor, indicating its strong electrophilicity. This implies that the C_{b1} in the cofactor is the most likely site to react with the negatively charged substrate (especially at the α,β-unsaturated C−C bond). From **React**, a transition state (**TS1**, Figure 3) for the cycloaddition between substrate and cofactor and the resultant pyrrolidine adduct (**Int1**, Figure 3) were optimized. In **TS1**, the key C_α−C_{b1} and C_β−C_{a6} distances are 2.00 and 2.83 Å, respectively. The **TS1** has been confirmed by frequency analysis to be a first-order saddle point with an imaginary frequency (379i cm^{-1}), which is corresponding to a vibrational mode involving a strong C_α−C_{b1} coupling and a relatively weaker C_β−C_{a6} coupling. The reoptimizations starting with slightly perturbed **TS1** structures always led to either **React** or **Int1**. All attempts to locate an intermediate with only one C−C bond formed between substrate and cofactor (C_α−C_{b1} or C_β−C_{a6}) failed. With the **TS1** structure as the starting point, the IRC (intrinsic reaction coordinate) calculations using the damped velocity verlet integrator (DVV, which is of high efficiency and stability for large and complex systems)[64] confirms that it is **TS1** that is the transition state to connect the **React** and **Int1** minima (see Figure S3 in the Supporting Information). These results indicate a 1,3-dipolar cycloaddition via **TS1** where the C_α−C_{b1} and C_β−C_{a6} bondings are concerted. The barrier for this step is calculated to be 14.3 kcal mol^{-1}, and the resulting pyrrolidine intermediate (**Int1**) lies 1.1 kcal mol^{-1} lower than the reactant complex of **React** (see Figure 5).

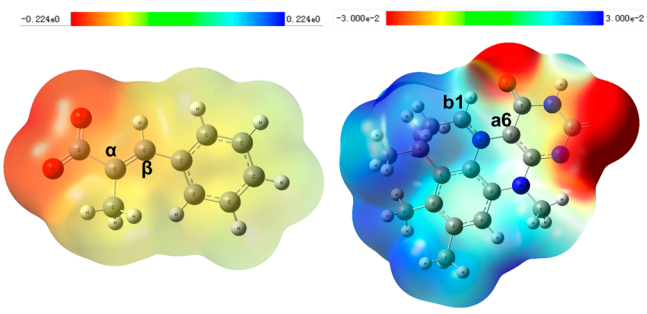

Figure 4. Electrostatic potentials mapped onto surfaces of total electron densities for the optimized substrate (left) and cofactor (right). The red and blue indicate the regions with higher and lower electron densities, respectively. Atom labels have been indicated in Figure 2.

In **Int1**, the C_α−C_β bond becomes saturated with a distance of 1.56 Å, 0.21 Å longer than that in **React** (1.35 Å) (Figure 3). The next step is the decarboxylation of the **Int1** pyrrolidine adduct (Figure 2). A corresponding transition state (**TS2**, Figure 3) has been located and computed to have an imaginary frequency of 233i cm^{-1}. It turns out that this is a concerted process where the decarboxylation is initiated by the C_β−C_{a6} bond dissociation with the C_α−CO_2 and C_β−C_{a6} distances being 1.94 and 2.73 Å in **TS2**, respectively. We could not obtain an intermediate with only one bond cleavage (C_α−CO_2 or C_β−C_{a6}). The subsequent IRC calculations show that it is **TS2** to connect **Int1** and **Int2** (Figure S4). This step is calculated to have a barrier of 14.8 kcal mol^{-1} and leads to a styrene derivative (**Int2**, Figure 3) in which the C_α−C_{b1} single bond (1.53 Å) is kept and the C_α−C_β interaction (1.35 Å) is retransformed to an unsaturated double bond from the single bond in **Int1** (1.56 Å).

With the formed CO_2 excluded from **Int2** and the Glu282 included, the complex was reoptimized (see **Int2b** in Figures 2 and 3). In the **Int2b** structure, the hydroxyl hydrogen of Glu282 (H_E) is positioned at a distance of 2.19 Å to the C_α atom. From **Int2b**, a transition state (**TS3**, Figure 3) has been found with an imaginary frequency of 944i cm^{-1}. In **TS3**, simultaneously with the C_α protonation by Glu282 (the distances of H_E to C_α and the Glu282 oxygen are 1.32 and 1.33 Å respectively), the C_β−C_{a6} bond is formed again to generate the second pyrrolidine adduct (see **Int3** in Figures 2 and 3) where the C_α−C_β bond distance is elongated to 1.56 Å from 1.35 Å in **Int2**. The IRC calculations also verify that **TS3** has a concerted character to connect **Int2b** and **Int3** (Figure S5). The barrier for this step is 14.3 kcal mol^{-1} (Figure 5).

The final step is the decomposition of the second pyrrolidine (i.e., **Int3**) via the concerted C_α−C_{b1} and C_β−C_{a6} bond dissociations to form the final styrene product (Figure 2). This kind of transition state (**TS4**) and product (**Prod**) have been optimized and given in Figure 3. **TS4** has an imaginary frequency of 427i cm^{-1} with the C_α−C_{b1} and C_β−C_{a6} distances being 2.02 and 2.65 Å respectively. Also, **TS4** has been proven

DOI: 10.1021/acs.joc.6b01872
J. Org. Chem. 2016, 81, 9289−9295

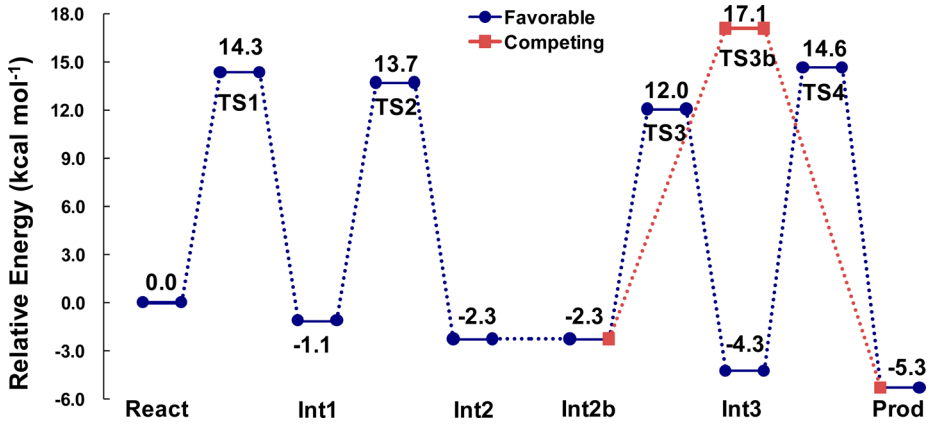

Figure 5. Potential energy profile for the Fdc1-catalyzed decarboxylation of α-methylcinnamic acid.

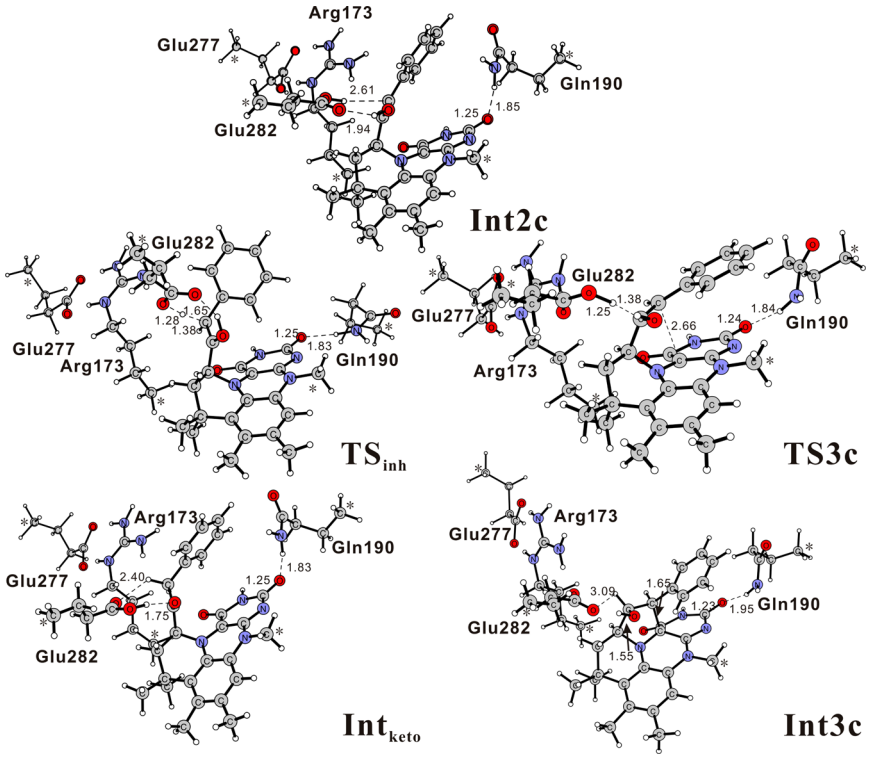

Figure 6. Optimized structures of key stationary points in the Fdc1 reaction with α-hydroxycinnamic acid. The **TS$_{inh}$** and **TS3c** have imaginary frequencies of 1286*i* and 1368*i* cm^{-1}, respectively.

to have the correct nature to connect **Int3** and **Prod** by the IRC calculations (Figure S6). This step is found to be rate-limiting in the overall reaction with a barrier of 18.9 kcal mol^{-1} (Figure 5), a value reasonably in line with the experimental reaction rate (k_{cat}) of 7.6 s^{-1} for the substrate of cinnamic acid.[12] The overall reaction is calculated to be slightly exothermic by 5.3 kcal mol^{-1}, making the reverse reaction (i.e., the CO_2 fixation) feasible with a barrier of 19.9 kcal mol^{-1} (Figure 5). The introduction of entropy to the energetics obtains the consistent conclusion in the forward reaction. For example, the overall energy barrier with entropy corrected in the forward direction is 20.1 kcal mol^{-1} also with the last step being rate-limiting (see Figure S1), to be compared to the nonentropy value of 18.9 kcal mol^{-1} (Figure 5). However, the reverse barrier with the estimated entropy included is somewhat high by 26.0 kcal mol^{-1} (Figure S1). Considering the absence of the experimental reverse reaction rate and the uncertainty of entropy calculations, it is difficult to assess the reasonability of such a reverse barrier. At present, it is probably inappropriate to use this reverse barrier to rule out the mechanism calculated here.

In the reversible Fdc1 reaction, the novel PrFMN cofactor plays several significant roles. The prenyl moiety in the cofactor acts as the crucial electrophile to initiate the cycloaddition with the substrate α,β-unsaturated bond, rendering the necessity of the prenylation of flavin mononucleotide (FMN) and the uniqueness of PrFMN. The flavin moiety functions as an electron reservoir to delocalize the charges developing during the reaction, which can be reflected by the elastic change of the C_{a3}–O_{a2} bond distance (shown in Figure 2) that is shortened to 1.23 Å in **Int1** from 1.24 Å in **React**, then elongated to 1.25 Å in **Int2**, shortened again to 1.23 Å in **Int3**, and finally elongated back to 1.24 Å in **Prod** (Figure 3). This is consistent with the change of the O_{a2} charge (see Table S1 in the

DOI: 10.1021/acs.joc.6b01872
J. Org. Chem. 2016, 81, 9289–9295

Supporting Information for the Mulliken charges at the O_{a2} atom). Meanwhile, the distance of the Gln190 hydrogen to the O_{a2} atom makes a corresponding elastic change (1.87, 1.97, 1.83, 2.00, and 1.87 Å in **React**, **Int1**, **Int2**, **Int3**, and **Prod**, respectively, Figure 3), indicating that the Gln190 plays an important role in stabilizing the developing negative charges at the O_{a2} atom through hydrogen bonding. Finally, the flavin plane may assist in the substrate orientation via π-stacking interactions.

From the styrene derivative (i.e., **Int2b**), we also obtained a transition state (**TS3b**, given in Figure S7 in the Supporting Information) for the **Int2b** decomposition, where the C_α–C_{b1} bond cleavage is concomitant with the C_α protonation by the Glu282, directly leading to the final styrene product (i.e., **Prod**). Although this pathway (the red curve in Figure 5) is feasible in the forward direction with a barrier of 19.4 kcal mol^{-1} (to be compared to the barrier of 18.9 kcal mol^{-1} in the pathway via **TS3** and **TS4**, i.e., the blue curve in Figure 5), its reverse barrier is somewhat high (22.4 kcal mol^{-1}). The inclusion of entropy decreases the barrier differences between the two pathways (see the red and blue curves in Figure S1). Therefore, this pathway via **TS3b** may be a little unfavorable but still competing.

The Inhibition of Fdc1 by α-Hydroxycinnamic Acid. It was found that Fdc1 was reversibly inhibited by α-hydroxycinnamic acid leading to a covalent inhibitor–cofactor adduct (see $\mathbf{Int_{keto}}$ in Figure 2), which has been characterized to be a ketone intermediate by X-ray crystallography (PDB: 4ZA9).[12] This inhibition was speculated to be attributed to the tautomerization from an enol intermediate (see **Int2c** in Figure 2, corresponding to the **Int2b** styrene derivative) to a ketone (denoted by $\mathbf{Int_{keto}}$ in Figure 2). We have optimized the enol (**Int2c**) and ketone ($\mathbf{Int_{keto}}$) intermediates (Figure 6) and located a transition state connecting them ($\mathbf{TS_{inh}}$, Figure 6), which has been verified by the IRC calculations (Figure S8). It is very interesting to find that, in $\mathbf{TS_{inh}}$, the Glu282 works as a proton transporter to abstract the hydroxyl proton and donate its proton to the C_β atom. The ketone formation through $\mathbf{TS_{inh}}$ has a low barrier of 7.4 kcal mol^{-1} with an exothermicity of 7.9 kcal mol^{-1} (Figure 7). This means that the tautomerization from enol to ketone is very fast and the reverse conversion is energetically accessible but much slower.

From the **Int2c** enol, we also obtained a transition state (**TS3c**, Figure 6) for the formation of a pyrrolidine adduct (see **Int3** in Figure 2 and **Int3c** in Figure 6). In **TS3c**, the Glu282 only serves as a proton donor to protonate the C_α atom (instead of C_β in $\mathbf{TS_{inh}}$) resulting in the C_β–C_{a6} bonding, like the third step of second pyrrolidine formation in the case of α-methylcinnamic acid. By the IRC calculations (Figure S9), **TS3c** has been confirmed to connect the correct minima (**Int2c** and **Int3c**). However, the barrier for pyrrolidine formation via **TS3c** (14.6 kcal mol^{-1}) is 7.2 kcal mol^{-1} higher than the tautomerization to ketone via $\mathbf{TS_{inh}}$ (Figure 7). This strongly demonstrates that, when α-hydroxycinnamic acid is used, the catalysis is energetically unfavorable and the Fdc1 enzyme should be inhibited to a stable ketone species with the assistance of Glu282 in the proton transportation from hydroxyl to C_β. It is worth mentioning that the inclusion of entropy in the energetics (see Figure S2) does not alter any conclusions about the reaction of Fdc1 with α-hydroxycinnamic acid.

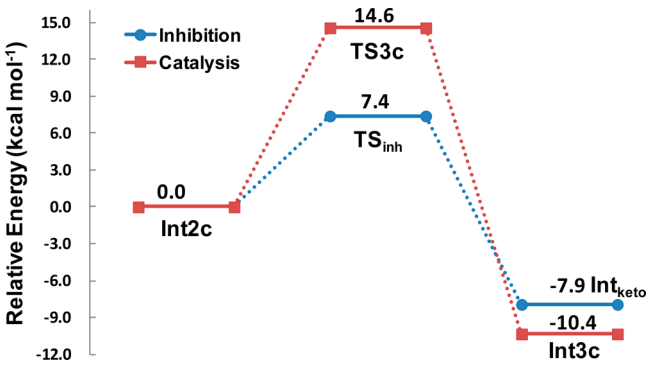

Figure 7. Key energetics for the Fdc1 reaction with α-hydroxycinnamic acid.

CONCLUSION

In summary, the calculations provide effective evidence for the hypothesized 1,3-dipolar cycloaddition mechanism in the Fdc1-catalyzed decarboxylation of α-methylcinnamic acid,[12] including the cycloaddition between the α,β-unsaturated bond and the cofactor of prenylated flavin mononucleotide (PrFMN), the decarboxylation of the resultant pyrrolidine adduct leading to a styrene derivative, the formation of a second pyrrolidine species through the C_α protonation by Glu282, and the decomposition of the second pyrrolidine to form the final styrene product (Figure 2). The overall barrier is 18.9 kcal mol^{-1} with the last step being rate-limiting. Both prenyl and flavin moieties in PrFMN play significant roles in the catalysis. Furthermore, it is found that the neutral Glu282 residue has two faces during catalysis or inhibition, accompanied by the C_α or C_β atom as a proton acceptor. When α-hydroxycinnamic acid is used, the Glu282 transports the proton from the hydroxyl to C_β to promote the tautomerization from an enol intermediate to a ketone species leading to the inhibition of the Fdc1 enzyme, rather than purely donating its proton to C_α to produce styrene (unlike the reaction of α-methylcinnamic acid). The results here advance the understanding of the particularly novel PrFMN cofactor and expand insights into the roles of vitamin B2 and glutamic acid in enzymatic decarboxylation, inspiring related enzyme engineering and organic synthesis aiming at optimizing decarboxylation efficiency.

ASSOCIATED CONTENT

Supporting Information

The Supporting Information is available free of charge on the ACS Publications website at DOI: 10.1021/acs.joc.6b01872.

Entropy-corrected energetics for the reactions with α-methylcinnamic acid and α-hydroxycinnamic acid, IRC results for **TS1**, **TS2**, **TS3**, **TS4**, $\mathbf{TS_{inh}}$, and **TS3c**, optimized structure of **TS3b**, Mulliken charges at the O_{a2} atom, and Cartesian coordinates of all optimized structures (PDF)

AUTHOR INFORMATION

Corresponding Author

*E-mail: shlchen@bit.edu.cn.

Notes

The authors declare no competing financial interest.

DOI: 10.1021/acs.joc.6b01872
J. Org. Chem. 2016, 81, 9289–9295

■ ACKNOWLEDGMENTS

This work was financially supported by the National Natural Science Foundation of China (21373027), Beijing Nova Program (Z151100000315055), and the 111 Project (B07012).

■ REFERENCES

(1) Kourist, R.; Guterl, J. K.; Miyamoto, K.; Sieber, V. *ChemCatChem* **2014**, *6*, 689−701.
(2) McKenna, R.; Nielsen, D. R. *Metab. Eng.* **2011**, *13*, 544−554.
(3) Edlin, D. A. N.; Narbad, A.; Gasson, M. J.; Dickinson, J. R.; Lloyd, D. *Enzyme Microb. Technol.* **1998**, *22*, 232−239.
(4) Richard, P.; Viljanen, K.; Penttila, M. *AMB Express* **2015**, *5*, 12.
(5) Mukai, N.; Masaki, K.; Fujii, T.; Kawamukai, M.; Iefuji, H. *J. Biosci. Bioeng.* **2010**, *109*, 564−569.
(6) Lin, F.; Ferguson, K. L.; Boyer, D. R.; Lin, X. N.; Marsh, E. N. G. *ACS Chem. Biol.* **2015**, *10*, 1137−1144.
(7) Zhang, H.; Javor, G. T. *J. Bacteriol.* **2000**, *182*, 6243−6246.
(8) Jacewicz, A.; Izumi, A.; Brunner, K.; Schnell, R.; Schneider, G. *PLoS One* **2013**, *8*, e63161.
(9) Liu, J.; Liu, J. H. *Acta Biochim. Biophys. Sin.* **2006**, *38*, 725−730.
(10) Bentinger, M.; Tekle, M.; Dallner, G. *Biochem. Biophys. Res. Commun.* **2010**, *396*, 74−79.
(11) Aussel, L.; Pierrel, F.; Loiseau, L.; Lombard, M.; Fontecave, M.; Barras, F. *Biochim. Biophys. Acta, Bioenerg.* **2014**, *1837*, 1004−1011.
(12) Payne, K. A.; White, M. D.; Fisher, K.; Khara, B.; Bailey, S. S.; Parker, D.; Rattray, N. J. W.; Trivedi, D. K.; Goodacre, R.; Beveridge, R.; Barran, P.; Rigby, S. E. J.; Scrutton, N. S.; Hay, S.; Leys, D. *Nature* **2015**, *522*, 497−501.
(13) Clarke, C. F.; Allan, C. M. *Nature* **2015**, *522*, 427−428.
(14) White, M. D.; Payne, K. A.; Fisher, K.; Marshall, S. A.; Parker, D.; Rattray, N. J. W.; Trivedi, D. K.; Goodacre, R.; Rigby, S. E. J.; Scrutton, N. S.; Hay, S.; Leys, D. *Nature* **2015**, *522*, 502−506.
(15) Lee, C.; Yang, W.; Parr, R. G. *Phys. Rev. B: Condens. Matter Mater. Phys.* **1988**, *37*, 785−789.
(16) Becke, A. D. *J. Chem. Phys.* **1993**, *98*, 5648−5652.
(17) Becke, A. D. *J. Chem. Phys.* **1993**, *98*, 1372−1377.
(18) Pellissier, H. *Tetrahedron* **2007**, *63*, 3235−3285.
(19) Ess, D. H.; Houk, K. N. *J. Am. Chem. Soc.* **2008**, *130*, 10187−10198.
(20) Frisch, M. J.; Trucks, G. W.; Schlegel, H. B.; Scuseria, G. E.; Robb, M. A.; Cheeseman, J. R.; Scalmani, G.; Barone, V.; Mennucci, B.; Petersson, G. A.; Nakatsuji, H.; Caricato, M.; Li, X.; Hratchian, H. P.; Izmaylov, A. F.; Bloino, J.; Zheng, G.; Sonnenberg, J. L.; Hada, M.; Ehara, M.; Toyota, K.; Fukuda, R.; Hasegawa, J.; Ishida, M.; Nakajima, T.; Honda, Y.; Kitao, O.; Nakai, H.; Vreven, T.; Montgomery, J. A., Jr.; Peralta, J. E.; Ogliaro, F.; Bearpark, M.; Heyd, J. J.; Brothers, E.; Kudin, K. N.; Staroverov, V. N.; Keith, T.; Kobayashi, R.; Normand, J.; Raghavachari, K.; Rendell, A.; Burant, J. C.; Iyengar, S. S.; Tomasi, J.; Cossi, M.; Rega, N.; Millam, J. M.; Klene, M.; Knox, J. E.; Cross, J. B.; Bakken, V.; Adamo, C.; Jaramillo, J.; Gomperts, R.; Stratmann, R. E.; Yazyev, O.; Austin, A. J.; Cammi, R.; Pomelli, C.; Ochterski, J. W.; Martin, R. L.; Morokuma, K.; Zakrzewski, V. G.; Voth, G. A.; Salvador, P.; Dannenberg, J. J.; Dapprich, S.; Daniels, A. D.; Farkas, O.; Foresman, J. B.; Ortiz, J. V.; Cioslowski, J.; Fox, D. J. *Gaussian 09*, Revision D.01; Gaussian: Wallingford, CT, USA, 2013.
(21) Hehre, W. J.; Ditchfield, R.; Pople, J. A. *J. Chem. Phys.* **1972**, *56*, 2257−2261.
(22) Francl, M. M.; Pietro, W. J.; Hehre, W. J.; Binkley, J. S.; Gordon, M. S.; Defrees, D. J.; Pople, J. A. *J. Chem. Phys.* **1982**, *77*, 3654−3665.
(23) Barone, V.; Cossi, M. *J. Phys. Chem. A* **1998**, *102*, 1995−2001.
(24) Cammi, R.; Mennucci, B.; Tomasi, J. *J. Phys. Chem. A* **1999**, *103*, 9100−9108.
(25) Klamt, A.; Schüürmann, G. *J. Chem. Soc., Perkin Trans. 2* **1993**, 799−805.
(26) Tomasi, J.; Mennucci, B.; Cammi, R. *Chem. Rev.* **2005**, *105*, 2999−3093.
(27) Blomberg, M. R.; Borowski, T.; Himo, F.; Liao, R.-Z.; Siegbahn, P. E. M. *Chem. Rev.* **2014**, *114*, 3601−3658.
(28) Himo, F.; Siegbahn, P. E. M. *Chem. Rev.* **2003**, *103*, 2421−2456.
(29) Siegbahn, P. E. M. *Q. Rev. Biophys.* **2003**, *36*, 91−145.
(30) Siegbahn, P. E. M.; Blomberg, M. R. A.; Chen, S.-L. *J. Chem. Theory Comput.* **2010**, *6*, 2040−2044.
(31) Liu, Y.-F.; Yu, J.-G.; Siegbahn, P. E. M.; Blomberg, M. R. A. *Chem. - Eur. J.* **2013**, *19*, 1942−1954.
(32) Chen, S.-L.; Blomberg, M. R. A.; Siegbahn, P. E. M. *J. Phys. Chem. B* **2011**, *115*, 4066−4077.
(33) Hirao, H. *J. Phys. Chem. A* **2011**, *115*, 9308−9313.
(34) Zhang, H.-M.; Chen, S.-L. *J. Chem. Theory Comput.* **2015**, *11*, 2525−2535.
(35) Grimme, S. *J. Comput. Chem.* **2004**, *25*, 1463−1473.
(36) Grimme, S. *J. Comput. Chem.* **2006**, *27*, 1787−1799.
(37) Grimme, S.; Antony, J.; Ehrlich, S.; Krieg, H. *J. Chem. Phys.* **2010**, *132*, 154104.
(38) Goerigk, L.; Grimme, S. *Phys. Chem. Chem. Phys.* **2011**, *13*, 6670−6688.
(39) Liao, R.-Z.; Thiel, W. *J. Phys. Chem. B* **2013**, *117*, 3954−3961.
(40) Chen, S.-L.; Fang, W.-H.; Himo, F. *Theor. Chem. Acc.* **2008**, *120*, 515−522.
(41) Siegbahn, P. E. M. *J. Comput. Chem.* **2001**, *22*, 1634−1645.
(42) Siegbahn, P. E. M.; Blomberg, M. R. A. *Chem. Rev.* **2010**, *110*, 7040−7061.
(43) Siegbahn, P. E. M. *JBIC, J. Biol. Inorg. Chem.* **2006**, *11*, 695−701.
(44) Himo, F. *Theor. Chem. Acc.* **2006**, *116*, 232−240.
(45) Siegbahn, P. E.; Himo, F. *JBIC, J. Biol. Inorg. Chem.* **2009**, *14*, 643−651.
(46) Sevastik, R.; Himo, F. *Bioorg. Chem.* **2007**, *35*, 444−457.
(47) Alberto, M. E.; Leopoldini, M.; Russo, N. *Inorg. Chem.* **2011**, *50*, 3394−3403.
(48) Ribeiro, A. J. M.; Alberto, M. E.; Ramos, M. J.; Fernandes, P. A.; Russo, N. *Chem. - Eur. J.* **2013**, *19*, 14081−14089.
(49) Marino, T.; Russo, N.; Toscano, M. *Chem. - Eur. J.* **2013**, *19*, 2185−2192.
(50) Leopoldini, M.; Russo, N.; Toscano, M. *J. Am. Chem. Soc.* **2007**, *129*, 7776−7784.
(51) Leopoldini, M.; Russo, N.; Toscano, M.; Dulak, M.; Wesolowski, T. A. *Chem. - Eur. J.* **2006**, *12*, 2532−2541.
(52) Amata, O.; Marino, T.; Russo, N.; Toscano, M. *J. Am. Chem. Soc.* **2009**, *131*, 14804−14811.
(53) Sousa, S. F.; Fernandes, P. A.; Ramos, M. J. *J. Am. Chem. Soc.* **2007**, *129*, 1378−1385.
(54) Cerqueira, N. M. F. S. A.; Fernandes, P. A.; Eriksson, L. A.; Ramos, M. J. *Biophys. J.* **2006**, *90*, 2109−2119.
(55) Bushnell, E. A. C.; Gherib, R.; Gauld, J. W. *J. Phys. Chem. B* **2013**, *117*, 6701−6710.
(56) Liu, H.; Llano, J.; Gauld, J. W. *J. Phys. Chem. B* **2009**, *113*, 4887−4898.
(57) Huang, W. J.; Llano, J.; Gauld, J. W. *J. Phys. Chem. B* **2010**, *114*, 11196−11206.
(58) Erdtman, E.; Bushnell, E. A. C.; Gauld, J. W.; Eriksson, L. A. *J. Phys. Chem. B* **2010**, *114*, 16860−16870.
(59) Robinet, J. J.; Gauld, J. W. *J. Phys. Chem. B* **2008**, *112*, 3462−3469.
(60) Li, H.; Robertson, A. D.; Jensen, J. H. *Proteins: Struct., Funct., Genet.* **2005**, *61*, 704−721.
(61) Bas, D. C.; Rogers, D. M.; Jensen, J. H. *Proteins: Struct., Funct., Genet.* **2008**, *73*, 765−783.
(62) Olsson, M. H. M.; Søndergaard, C. R.; Rostkowski, M.; Jensen, J. H. *J. Chem. Theory Comput.* **2011**, *7*, 525−537.
(63) Sondergaard, C. R.; Olsson, M. H. M.; Rostkowski, M.; Jensen, J. H. *J. Chem. Theory Comput.* **2011**, *7*, 2284−2295.
(64) Hratchian, H. P.; Schlegel, H. B. *J. Phys. Chem. A* **2002**, *106*, 165−169.

DOI: 10.1021/acs.joc.6b01872
J. Org. Chem. 2016, 81, 9289−9295